Marbled texture of sputtered Al/Si alloy thin film on Si

Marbled texture of sputtered Al/Si alloy thin film on Si

M.G. Gentile[1,2], J.A. Muñoz-Tabares[3], A. Chiodoni[3], C. Sgorlon[2], I. Para[2], R. Carta[2], G. Richieri[2], K. Bejtka[3], L. Merlin[2], E. Vittone[1]

[1] Physics Department and NIS Interdepartmental Center, University of Torino, via P. Giuria 1, 10125 Torino.

[2] Vishay Semiconductor Italiana S.p.A., via Liguria 49 10071 Borgaro, Italy.

[3] Istituto Italiano di Tecnologia, Center for Space Human Robotics, Corso Trento 21, 10129 Torino, Italy.

Abstract

DC magnetron sputtering is a commonly used technique for the fabrication of silicon based electronic devices, since it provides high deposition rates and uniform large area metallization. However, in addition to the thickness uniformity, coating optical uniformity is a crucial need for semiconductor industrial processes, due to the wide use of optical recognition tools.

In the silicon-based technology, aluminum is one of the most used materials for the metal contact. Both the pre-deposition substrate cleaning and the sputtering conditions determine the quality and the crystalline properties of the final Al deposited film. In this paper is shown that not all the mentioned conditions lead to good quality and uniform Al films. In particular, it is shown that under certain standard process conditions, Al/Si alloy (1% Si) metallization on a [100] Si presents a non-uniform reflectivity, with a marbled texture caused by flakes with milky appearance. This optical inhomogeneity is found to be caused by the coexistence of randomly orient Al/Si crystal, with heteroepitaxial Al/Si crystals, both grown on Si substrate. Based on the microstructural analysis, some strategies to mitigate or suppress this marbled texture of the Al thin film are proposed and discussed.

Keywords

Silicon, Al/Si thin film deposition, heteroepitaxy, sputtering, surface roughness, light scattering, TEM, XRD

1. Introduction

Aluminum is a widely used metal both as primary interconnect material in integrated circuits and as forming ohmic (to p-type silicon region and to heavily-doped n regions) or rectifying contacts (to lightly doped n regions) in discrete silicon devices (e.g. diodes or transistors) [1].

In addition to the properties of the material (namely conductivity, overall processability, good adherence to the silicon dioxide surface, easy to be patterned), which make aluminum ideal for silicon metallization, the variety of Physical (PVD) and Chemical (CVD) Vapor Deposition techniques allow to achieve high productivity and reliability at industrial level.

Among PVD deposition techniques, DC magnetron sputtering is very popular in the semiconductor industry, because it allows the control of the metal layer composition, overcoming oxide formation problems associated with conventional sputtering, the thickness control accuracy and a high deposition rate [2]. Moreover, it allows the direct deposition of Al/Si alloys, which is the most commonly adopted method to inhibit the aluminum silicon interdiffusion at the contacts, causing junction spiking [3].

However, the polycrystalline structure of deposited Al films can influence the electronic properties of electronic devices, through atomic (electro or stress induced) migration along grain boundaries [4] [5] [6] [7].

The hetero-epitaxial growth of Al on Si is then required to avoid the inter-grain atomic diffusion. However, Al on Si hetero-epitaxy requires an accurate control of the deposition parameters to get

a uniform metal coverage over the entire Si wafer substrate and to ensure high product reliability especially for batch deposition.

During a systematic study aimed to individuate the optimal Al/Si deposition conditions to fabricate Si Schottky diodes, it was find an apparent marbled textured Al/Si film as shown in Fig. 1A. This photograph, taken under standard diffuse illumination conditions of the Al/Si layer deposited by DC magnetron sputtering on a 6" Si wafer, shows the presence of "milky" flakes, randomly dispersed throughout the wafer surface.

Although there is no evidence of remarkable effects on the electronic properties of the Al/Si contacts, this optical non-uniformity must be reduced not only for an aesthetic issue, since it can affect both the automatic alignment accuracy and critical size obtained during photolithographic processing [8].

To the best of our knowledge, this "marbled texture" has not been previously reported and explained. In this study, the results of different analyses are described and the correlation between the microstructure, surface roughness and crystal orientation with the optical reflectivity of the Al/Si alloy thin film are discussed. As an outcome, this study allowed the identification of experimental methods to control or to mitigate the optical non-uniformity of DC magnetron sputtered Al/Si thin films on silicon.

2. Experimental details

The substrates for Al/Si film deposition were 6" Czochralski [100] oriented p-type silicon wafers, with a resistivity of (28 ± 3) ohm·cm.

In order to remove the surface oxide, wafers were dip in aqueous HF ($3.7 \cdot 10^{-4}$ M) solution for 30 seconds [9]. After rinsing in de-ionized water and drying under nitrogen flow, the surface was H

terminated with hydrophobic property; the water contact angles were in the range of 60-70 degree.

Al/Si thin films were then sputtered on the substrates by DC magnetron sputtering process by using a commercial DC sputtering (Varian 3290) system.

In a typical process, each cleaned wafer was loaded into the preheating chamber, and pre-annealed at 623 K in Ar atmosphere. Then the substrate was transferred to the sputtering chamber and placed on a heater plate held at 473 K.

An aluminum silicon alloy sputtering target (Al/Si with 1% Si content), was used to deposit the Al/Si alloy film. The sputtering process was performed at 4.5 kW DC power in Ar atmosphere at gas partial pressure of 0.4 Pa; the O content was < 0.2 ppm. The deposition rate was 50 nm/s, and the total Al/Si film thickness about 3 μm, which is typically required for high power device operation.

An Ocean Optics USB4000 spectrometer connected to a R200-7-VIS-NIR probe for specular or to an ISP-REF for diffuse reflectance measurements was used for the optical characterization of the surface.

Morphological analyses of the Al/Si deposited thin film were carried out with a ZEISS Auriga dual beam-field emission scanning electron microscope (Focused Ion Beam (FIB) – Field Emission Scanning Electron Microscopy (FESEM)). An Oxford Energy Dispersive X-ray detector has been used to check the chemical composition.

The interface between the Si substrate and the Al/Si film was analyzed with a FEI Tecnai F20ST Transmission Electron Microscope (TEM) operating at 200 kV. An electron transparent TEM specimen in cross section was prepared from the starting sample, by using FIB, operating at 30kV. Final polishing was accomplished at 2kV in order to reduce the ion beam damage on sample.

X-ray diffraction (XRD) analysis was carried out using a PANalytical X'Pert X-ray diffractometer with a Cu x-ray source (Kα λ = 1.54059 A) in the Bragg-Brentano configuration.

Atomic Force Microscopy (AFM) performed with XE-100 with XEI 1.8.0 software.

Finally, the effects of the sputtering temperature on the flake coverage was studied as function of the process temperature and correlated with the film stress measured with a Tencor Flexus Stress Analyzer FLX2320.

3. Results

Fig. 1B shows the specular and diffuse reflectance in the visible range of one region with flakes (denoted in the following as F region), using the surface without flakes (denoted in the following as noF region) as reference. Although the absolute value of the diffuse reflectance vary to a large extent due to the high optical inhomogeneity of the flakes (Fig. 1A), the spectra shown in Fig. 1B are representative of the general optical properties of the flakes, which present a milky aspect because of higher diffuse (and lower specular) reflectance with respect to the noF region.

The correlation between the surface roughness of the F and noF region and their optical properties can be inferred from Figs. 2A, B, where both optical (A) and FESEM (B) micrographs are reported. Actually, surface roughness causes light scattering of the film surfaces, making the reflection less specular in nature [10] [11]. The milky aspect of the region on the right side (F) is related to higher hillocks with respect to those visible on the left side (noF), as put in evidence by the AFM map reported in Fig. 2C. The boxplot in Fig. 2D summarizes the main morphological features: the pixel height distribution is wider in F than in noF area, as indexed by the different values of the root mean square (RMS) and of the peak to valley height (Rpv).

The presence of hillocks is commonly attributed to stress relief mechanisms in the growing layer, depending on process parameters (sputter power and working pressure) and film thickness

[12][13]. However, to the best of our knowledge, there are no previous reports on the macroscopic and visible to the naked eye morphological non-homogeneity reported in this study.

In order to investigate the microstructure of these two different regions, a thin lamella straddling the F and noF regions was prepared for TEM analysis by using the conventional FIB cutting method (Fig. 3a).

From Bright-Field TEM image (Fig. 3b) it was possible to observe that the substrate is, as expected, homogeneous without evidence of grain boundaries, indicating that it is a monocrystalline Si material. On the other hand, the noF region of the Al/Si layer consists of several structured crystals (denoted as I-V) arranged in alternating domains of two different widths (narrow with ~0.4 μm and broad with ~1.5 μm). Regarding the F region, denoted as grain VI, there is no evidence of different crystal domains and a single grain is observed.

Figure 4 shows the Selected Area Electron Diffraction (SAED) analysis on grains I-VI; the electron diffraction pattern of the Si substrate is reported as reference.

By indexing the substrate SEAD pattern (bottom part of Fig. 4), it was possible to identify the Si phase in [110] axis zone, with the [-220] vector parallel to the layer/substrate interface and the [002] vector perpendicular thereto.

Grains I, III and V were identified as Al/Si phase in [110] axis zone; the vectors [-220] and [002] are perpendicular and parallel to the layer/substrate interface (in the sample plane), respectively, with the unit cell rotated 90° counter-clockwise with respect to the Si one. Such orientation will be referred to hereafter as domain type A; Fig. 5A shows a scheme of this unit cells arrangement.

Regarding grains II and IV, they were indexed as Al phase in [001] zone axis; as for domain type A, the [-220] and [002] vectors are perpendicular and parallel to the film/substrate interface, respectively. However, with respect to domain type A, the c axis of grains II and IV is rotated 90° in

the plane of the interface so that the [002] vector coincides with the observation axis (perpendicular to the sample plane); this orientation will be hereafter referred as domain type B (Fig. 5B).

Finally, grain VI (located into the F region) was identified as Al phase in [011] axis zone and the [-220] vector changes from perpendicular to parallel to the interface, assuming the same orientation as the substrate (fig. 5C).

Noteworthy that, starting from the conditions in which the substrate was perfectly oriented in axis zone (with the observation axis parallel to [110] vector). The sample was tilted of ~3° in the α angle (tilt direction parallel to the interface) and ~2° in the β angle (tilt direction perpendicular to the interface), in order to align the observation axis to the grain VI axis zone. This misorientation was considerably higher than that required to align grains I-V, which was less than 1° for both (α and β) tilting angles

In order to analyze the crystallographic relationship between substrate and Al layer, High Resolution TEM (HRTEM) was performed at the (I and VI Al/Si grains)/substrate interface. The Fast Fourier Transform (FFT) patterns obtained from those images were indexed using the abovementioned crystallographic models.

Fig. 6a shows an HRTEM image of the substrate (bottom) and grain I (top) interface. As expected from SAED (Fig. 4), by indexing the FFT patterns, the Si phase is in [110] zone axis with the [-220] and the [002] vectors parallel and perpendicular to the layer/substrate interface, respectively; Grain I was identified as Al in [110] axis zone, where the unit cell is rotated 90° counter-clockwise with respect to the Si one.

The FFT of the interface, which is the result of the superposition of grain I and substrate reveals an hetero-epitaxial growth of Al phase, so that Al(002)//Si(220) (white circle), with a relatively small

(5.2%) mismatch between the Al(002) (d = 2.024 A) and the Si(220) (d = 1.920 A) interplanar spacing.

Figure 6b is a closer view of the interface between substrate and grain I. The coordinate system for each phase as well as a filtered image (half box) from the same area are also shown, in which the Si(220) and Al(002) inter-planar spacing are clearly visible. Fig. 6c shows the full filtered image of Fig. 6b by considering only the Al(002) and Si(220) spots. This image highlights the correspondence between Al(002) and Si(220) planes, as well as the presence of edge dislocations (T symbols, mainly in the substrate), which allow the strain energy associated with the lattice mismatch to be relieved.

Finally, Fig. 7 shows an HRTEM image of the interface between substrate (bottom image) and grain VI (top). From the FFTs taken from the white boxes, it was possible to identify, as expected, the same (as in Fig. 6a) axis zone (Si[110]) of the substrate. However, there is no evidence of any epitaxial relationship between the Si substrate and the Al layer; from the FFT, it was only possible to distinguish the Al(111) plane spacing.

The absence of heteroepitaxial growth can be justified both by the large mismatch (~25%) between the Al (2-22) (d=1.431 A) and the Si (220) (d=1.920 A) inter-planar spacing, and by the misalignment between their axes. Actually, as mentioned above, to carry out SAED analysis in the F region, the sample was tilted at azimuthal and polar angles remarkably larger than those used to align the grains (I-V) of the noF region.

The absence of heteroepitaxial growth in the F region was furtherly confirmed by the TEM analysis carried out on a second lamella extracted from this region. From the bright field image shown in Fig. 8, it is possible to observe two Al/Si grains. The substrate SAED was indexed in the same axis zone as in the previous lamella. However, in this case, none of the two Al/Si grains presented an

epitaxial relationship with the substrate. The grain 1 was identified as Al[120], with angle misorientations of α = 3.3° and β=0.6 with respect to the substrate axis zone; grain 2 was indexed as Al[345], with angle misorientations of α = 0.2° and β=1.5°.

The results obtained by TEM analysis about the different crystallographic structures of the F and noF zones were corroborated by X-ray diffraction analysis, which was carried out on a noF region and on an F region with a high density of flakes (Fig. 9).

All the diffractograms show a strong Si(400) reflection occurring at $2\theta \approx 69°$ due the alignment of the diffraction vector parallel to the [100] direction of the Si substrate, but different Al/Si orientations in the F and noF regions.

The diffractogram of the noF region (A), shows a dominant reflection related to Al(220) at ($2\theta \approx$ 65°), whereas in F region (B), other peaks appear at $2\theta \approx$ 38°, 78° and 82°, which have been identified as due to Al(111), Al(311) and Al(222), respectively.

In conclusion, both XRD and TEM analyses provided evidence that flakes are correlated to a random orientation of Al/Si crystals, whereas noF region is structured in crystals with an epitaxial relationship with the substrate and with the {220} planes parallel to the interface.

As a final comment, elemental analysis carried out by energy dispersive x-ray (EDX) spectroscopy (not show here) did not provide any evidence of different chemical composition between grains I and VI.

On the basis of the above analysis, two different strategies to suppress or mitigate the non-uniform reflectivity have been followed. The first approach was inspired by the work of Yokoyama et al. [5] [14] [15], who succeeded to grow Al(110) single crystal film on a misoriented Si(100) substrate. This effect was interpreted as due to the preferential alignment of Al(110) lattice units

close to the step edge direction, which act as the nucleation centers for the growth of the dominant domain.

According to the above mentioned deposition protocol, an Al/Si thin film has been deposited on a misoriented (100) Si substrate (4° off toward [011] direction).

Actually, the X-ray diffractogram shows only a dominant Al(220) reflection (Fig. 10), which is very similar to the diffractogram (Fig. 9A) taken on a noF region of a standard Al deposition on a Si(100) substrate. The optical inspection of the sample (inset in Fig. 10) shows a uniform reflectivity of the Al layer, which is in agreement with a uniform orientation of the Al/Si grains.

The second approach was based on the study of the effects of the growth temperature on the Al/Si layer reflectivity and crystal structure. Fig. 11 summarizes the main results of this study. As the substrate temperature increases, the flake density reduces and flakes disappear at temperatures higher than 600 K. The structure zone model [16] can provide a preliminary interpretation of this result: when the substrate temperature is higher than 0.5 T/T_m, where T_m is the melting point of the film material (933 K), the volumetric diffusion of adatoms promote the growth of equiaxed grains and re-crystallization. As in the previous case of misoriented Si substrate, the optical inspection of the processed wafer is sufficient to assume an epitaxial growth of Al/Si on Si, with the formation of a dominant orientation of the Al/Si grains.

This conclusion is furtherly corroborated by the analysis of the Al/Si film stress evaluated by using the Stoney's equation , which relates the biaxial modulus of the substrate, the thicknesses of the film and substrate, to the curvature radius of pre and post thin film deposition [17]. Fig. 11 shows the results of the analysis performed on the samples processed at different sputtering temperatures.

This result can be interpreted noticing that the behavior of stress as function of temperature is opposite to the flakes density. At high temperature, the Al/Si growth is epitaxial, there are no flakes, and the strong coupling between the film/substrate lattices induces a remarkable stress due to the large mismatch of thermal expansion coefficients (α) of the Al/Si layer and the Si substrate (α_{Al}=23.1 x 10^6 K^{-1} , α_{Si}=2.6 x 10^6 K^{-1}) [18]. As the sputtering temperature decreases, the formation of flakes, randomly oriented, decouples the Al/Si film/substrate lattices, allowing local relaxation and then a minor distortion of the Al/Si film.

4. Conclusions

This paper describes a systematic investigation of the "Marble texture" occurring in DC sputtered Al/Si thin film on a [100] oriented Si wafer. This effect consists in the presence of highly diffuse reflective regions, which lead to an apparent non-uniformity of the metallization.

Analyses carried out by Optical, FESEM and AFM microscopies highlighted a higher roughness of the milky flakes (F regions) in comparison with the noF region, which is caused by different orientation of the Al grains. XRD, TEM and SAED studies showed that in the F regions, the Al/Si grains are randomly oriented, whereas in the noF areas, heteroepitaxy of Al/Si on Si occurs with a little lattice mismatch (5.2%) and two different Al/Si crystallographic orientations, rotated 90° in the plane of the interface.

In order to suppress or mitigate this optical non-uniformity, two different strategies are proposed: the first consists in the use of a misoriented substrate, which promotes the growth of Al/Si film oriented along the step edge direction.

The second method deals with the increase of the sputtering temperature, which allows higher mobility of adatoms, favorings the Al heteroepitaxial growth and suppressing the growth of randomly oriented crystal. However, in this case, a remarkable increase of the film stress induced

by the mismatch of the two lattices and the large difference on thermal expansion coefficients of the Al/Si layer and Si substrate has been observed.

This study is of potential interest for semiconductor industrial applications, since the optical non-homogeneity could be an issue for tools with optical recognition like “pick and place” tools that can’t recognize variation on optical characteristics of the device, or exposure tools with optical alignment.

Acknowledgments

The authors are grateful to Vacirca Irene, El Baradai Nabil, Sanfilippo Carmelo, Crudelini Filippo, Di Santo Natale, Vissicchio Bartolo, Azzarone Pasquale of Vishay Semiconductor Italia for the technical support.

References

[1] H.C. Card, Aluminum-Silicon Schottky barriers and ohmic contacts in integrated circuits, Electron Devices, IEEE Trans. 23 (1976) 538–544, doi: 10.1109/T-ED.1976.18449.

[2] T.J. Garosshen, T.A. Stephenson, T.P. Slavin, Aluminum Metallization Technology for Semiconductor Devices, Journal of Metals, 37 (1985) 55-59, doi: 10.1007/BF03257742.

[3] D. Widmann, H. Mader, H. Friedrich, Technology of Integrated Circuits, Springer Science & Business Media 2013.

[4] Y. Nakajima, K. Kusuyama, H. Yamaguchi, Y. Murakami, Growth of Single-Crystal Aluminum Films on Silicon Substrates by DC Magnetron Sputtering , Jpn. J. Appl. Phys. (1992) 1860–1867, doi: 10.1143/JJAP.31.1860.

[5] S. Yokoyama, H. Ichikawa, M. Koyanagi, Influence of sputtering geometry on crystallinity of Al(110) thin films on offset (100)Si, Japanese J. Appl. Physics, Part 1 Regul. Pap. Short Notes Rev. Pap. 32 (1993) 283–286, doi:10.1143/JJAP.32.L283.

[6] K. Kusaka, T. Hanabusa, M. Nishida, F. Inoko, Residual stress and in-situ thermal stress measurement of aluminum film deposited on silicon wafer, Thin Solid Films. 290-291 (1996) 248–253, doi: 10.1016/S0040-6090(96)09056-6.

[7] S. Yokoyama, K. Okamoto, Single-Crystal Growth of Al (110) on Vicinal Si (100) in Ultra-High-Vacuum Sputtering System, Jpn. J. Appl. Phys. 30 (1991) 3685–3690.

[8] R.J. Wilson, B.L. Weiss, The specular reflectivity of DC magnetron sputtered Al-1-percent Si films, Vacuum,42 (1991), 15, 987-994, doi: 10.1016/0042-207X(91)90005-4.

[9] Werner Kern, Handbook of semiconductor wafer cleaning technology, Noyes Publication, New Jersey, 1993.

[10] S.D. Kim, J.K. Rhee, I.S. Hwang, H.M. Park, H.C. Park, Surface condition effects of the inter-metal dielectrics on interconnect aluminum film properties, Thin Solid Films. 401 (2001) 273–278, doi: 10.1016/S0040-6090(01)01477-8.

[11] C. Kylner, L. Mattsson, Enhanced optical performance of aluminum films by copper inclusion, Thin Solid Films. 348 (1999) 222–226, doi: 10.1016/S0040-6090(98)01398-4.

[12] D. Resnik, J. Kovac, M. Godec, D. Vrtacnik, M. Mozek, S. Amon, The influence of target composition and thermal treatment on sputtered Al thin films on Si and SiO2 substrates, Microelectronic Engineering, 96 (2012), 29-35, doi: 10.1016/j.mee.2012.02.048.

[13] Soo-Jung Hwang, W. D. Nix, Young-Chang Joo, A model for hillock growth in Al thin films controlled by plastic deformation, Acta Materialia 55 (2007) 5297–5301, doi: 10.1016/j.actamat.2007.05.046.

[14] S. Yokoyama, H. Ichikawa, Y. Ichikawa, M. Koyanagi, Effects of hydrogen and bias on single-crystal Al growth on vicinal Si by DC magnetron sputtering, Japanese J. Appl.

Physics, Part 1 Regul. Pap. Short Notes Rev. Pap. 33 (1994) 459–461, doi: 10.1143/JJAP.33.459.

[15] S. Yokoyama, H. Ichikawa, M. Koyanagi, Influence of sputtering geometry on crystallinity of Al(110) thin films on offset (100)Si, Japanese J. Appl. Physics, Part 1 Regul. Pap. Short Notes Rev. Pap. 32 (1993) 283–286, doi: 10.1143/JJAP.32.L283.

[16] G.C.A.M. Janssen, M.M. Abdalla, F. van Keulen, B.R. Pujada, B. van Venrooy, Celebrating the 100th anniversary of the Stoney equation for film stress: Developments from polycrystalline steel strips to single crystal silicon wafers, Thin Solid Films. 517 (2009) 1858–1867, doi: 10.1016/j.tsf.2008.07.014.

[17] X. Feng, Y. Huang, a. J. Rosakis, On the Stoney Formula for a Thin Film/Substrate System With Nonuniform Substrate Thickness, J. Appl. Mech. 74 (2007) 1276, doi: 10.1115/1.2745392.

[18] E. Eiper, R. Resel, C. Eisenmenger-Sittner, M. Hafok , J. Keckes Thermally-induced stresses in thin aluminum layers grown on silicon. Powder Diffraction, 19 (2004) 74-76, doi: 10.1154/1.1649326.

Figure Captions

Fig 1. (A): Photograph of Al/Si film sputtered on a 6” Si wafer with marbled texture. (B) Specular and Diffuse reflectance spectra in the visible range of the F region, using the noF region as the reference.

Fig. 2: Optical (A) and FESEM (B) micrographs of the same region of the Al/Si deposited thin film. (C) AFM map (D) box-plots of the pixel height distributions of the two regions: RMS= (16 nm)/(13 nm); Rpv=(155 nm)/(142 nm) for F and noF regions, respectively.

Fig. 3: a) FESEM image of Al/Si film the white rectangle represents the area selected for the TEM lamella preparation; b) Bright Field-TEM image of the lamella extracted from the interface (dotted line) of the noF (left side) and F (right side) regions.

Fig. 4: SAED relevant to grains I-VI (top) and of the Si substrate (bottom); each pattern shows the labels that identify the crystallographic plane belonging to each spot, the phase and its zone axis, as well as a schematic drawing of the until cell with its orientation in the real space.

Fig. 5: 3D representation of the three domain types. The cubes on top represent Al unit cells lying on the Si substrate at the bottom; the crystallographic axis orientations refer to Fig. 4

Fig.6: a) HRTEM image of the substrate and grain I (see fig. 4) interface. White boxes indicate the areas from where the FFTs (right side) were taken; b) details of HRTEM image of the (grain I)/substrate interface, with the coordinate system for each phase; the half box on the right side is the filtered image; c) full filtered image of b) by considering the planes perpendicular to the interface; the symbol T indicates the presence of edge dislocations.

Fig. 7: a) HRTEM image of interface between substrate and grain VI. The FFT patterns are extracted from the rectangular regions.

Fig. 8: Bright Field-TEM image of a second lamella extracted from the F region.

Fig. 9: X-ray diffractograms of noF (A) and F (B) regions.

Fig. 10: X-ray diffractogram relevant to the Al deposition on a misoriented Si substrate. The inset shows the optical image of the sample.

Fig. 11: Wafer appearance and stress value for wafers processed at different substrate temperatures.

Fig1

Click here to download high resolution image

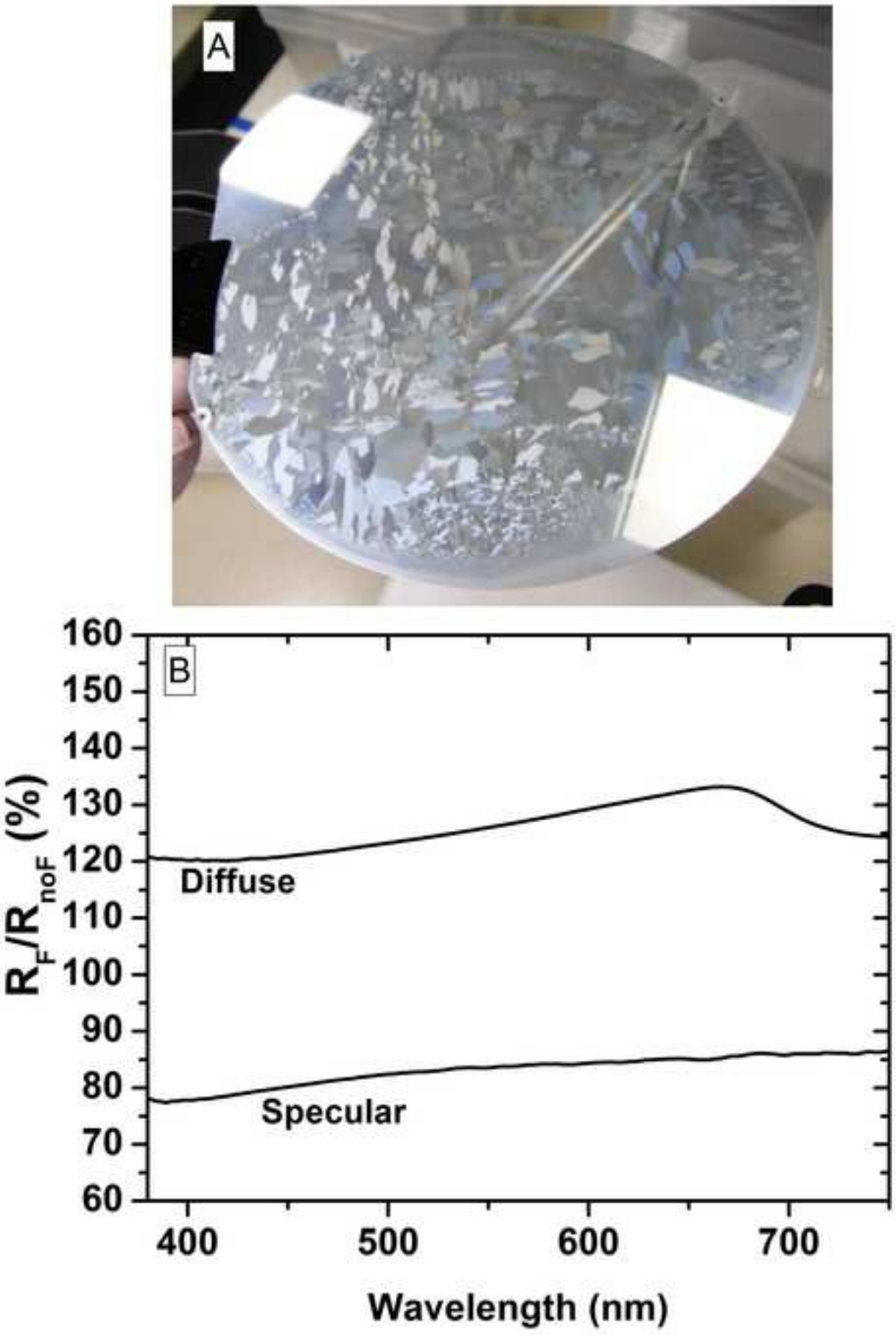

Fig2

Click here to download high resolution image

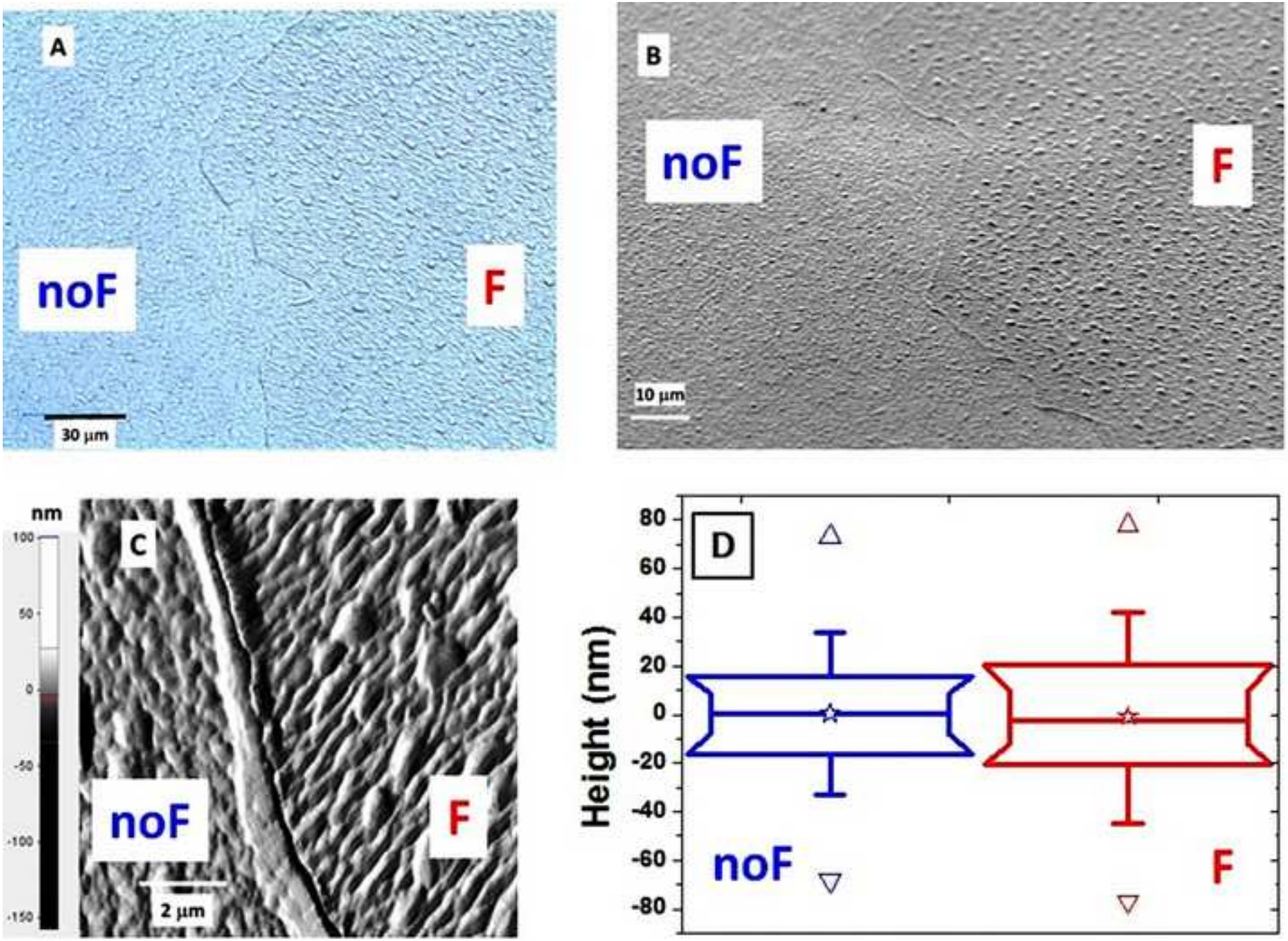

Fig3

Click here to download high resolution image

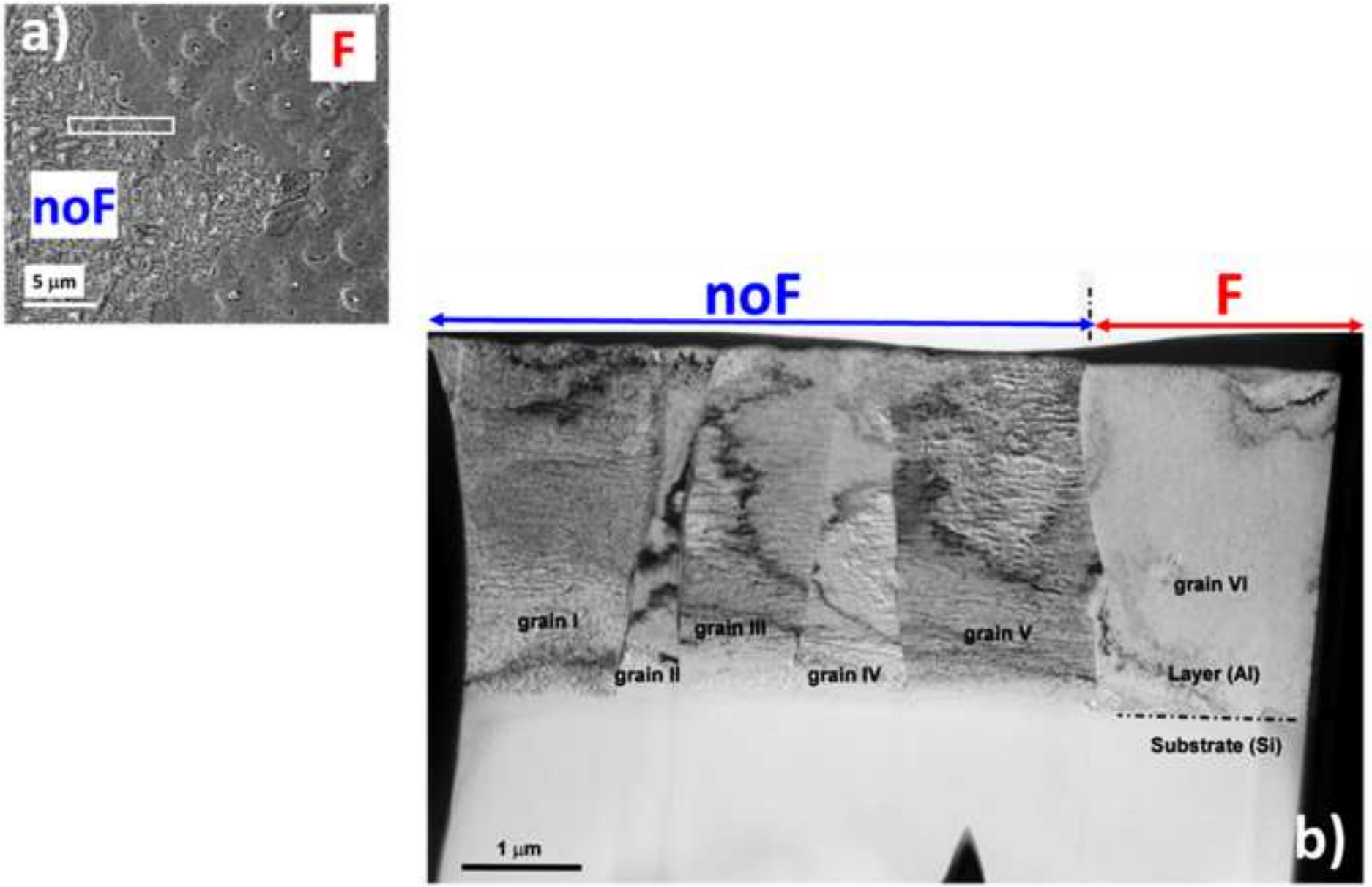

Fig4

Click here to download high resolution image

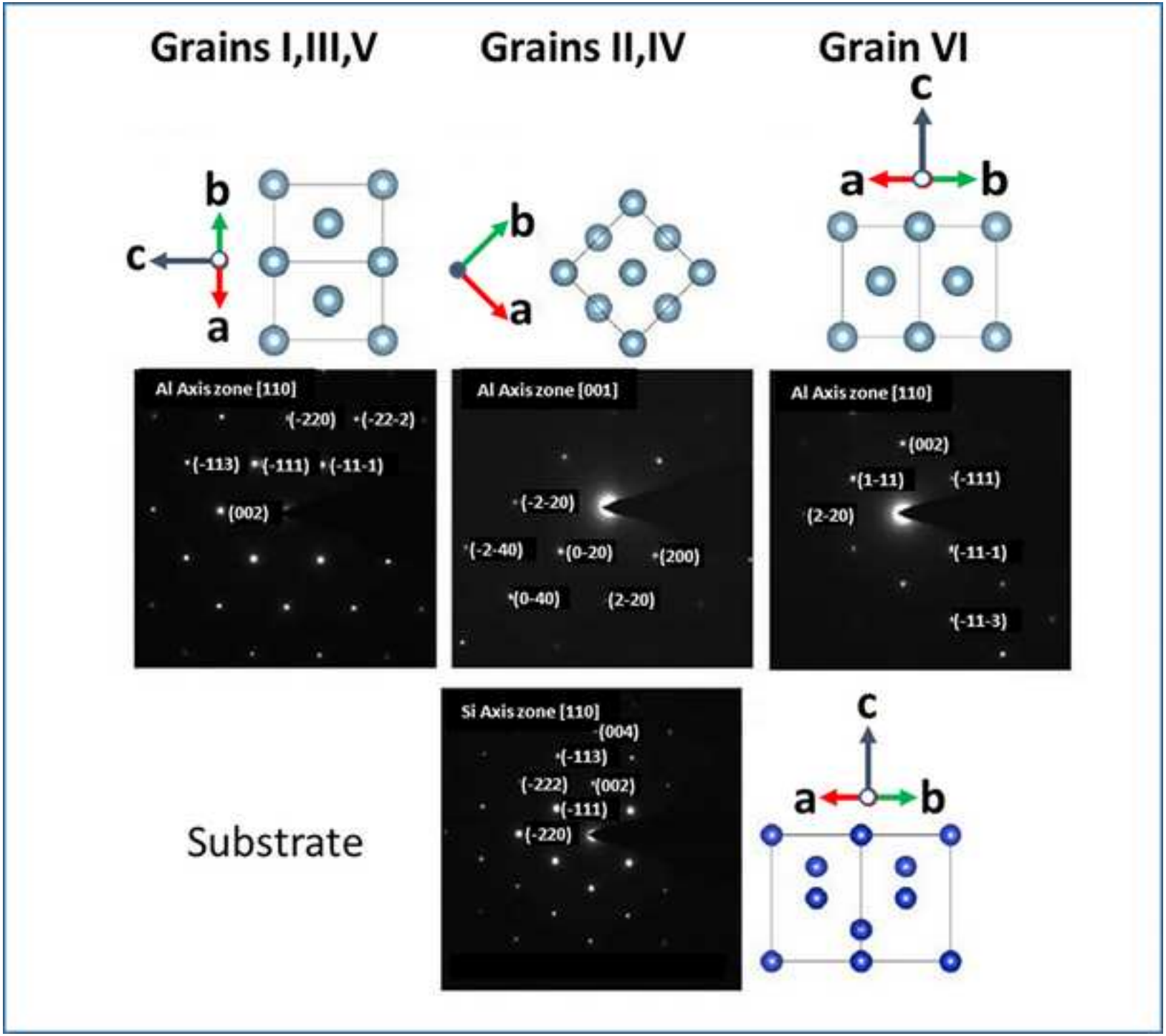

Fig5

Click here to download high resolution image

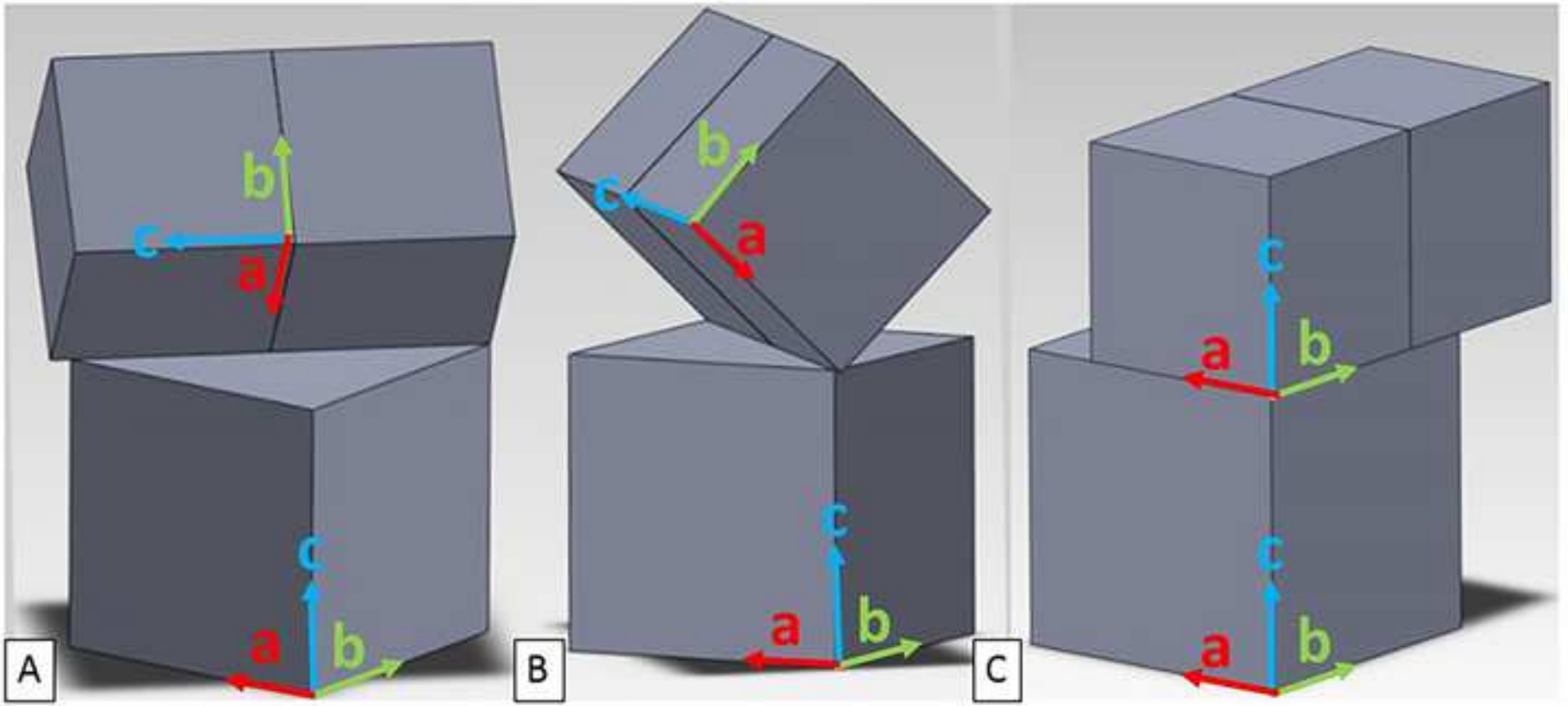

Fig6

Click here to download high resolution image

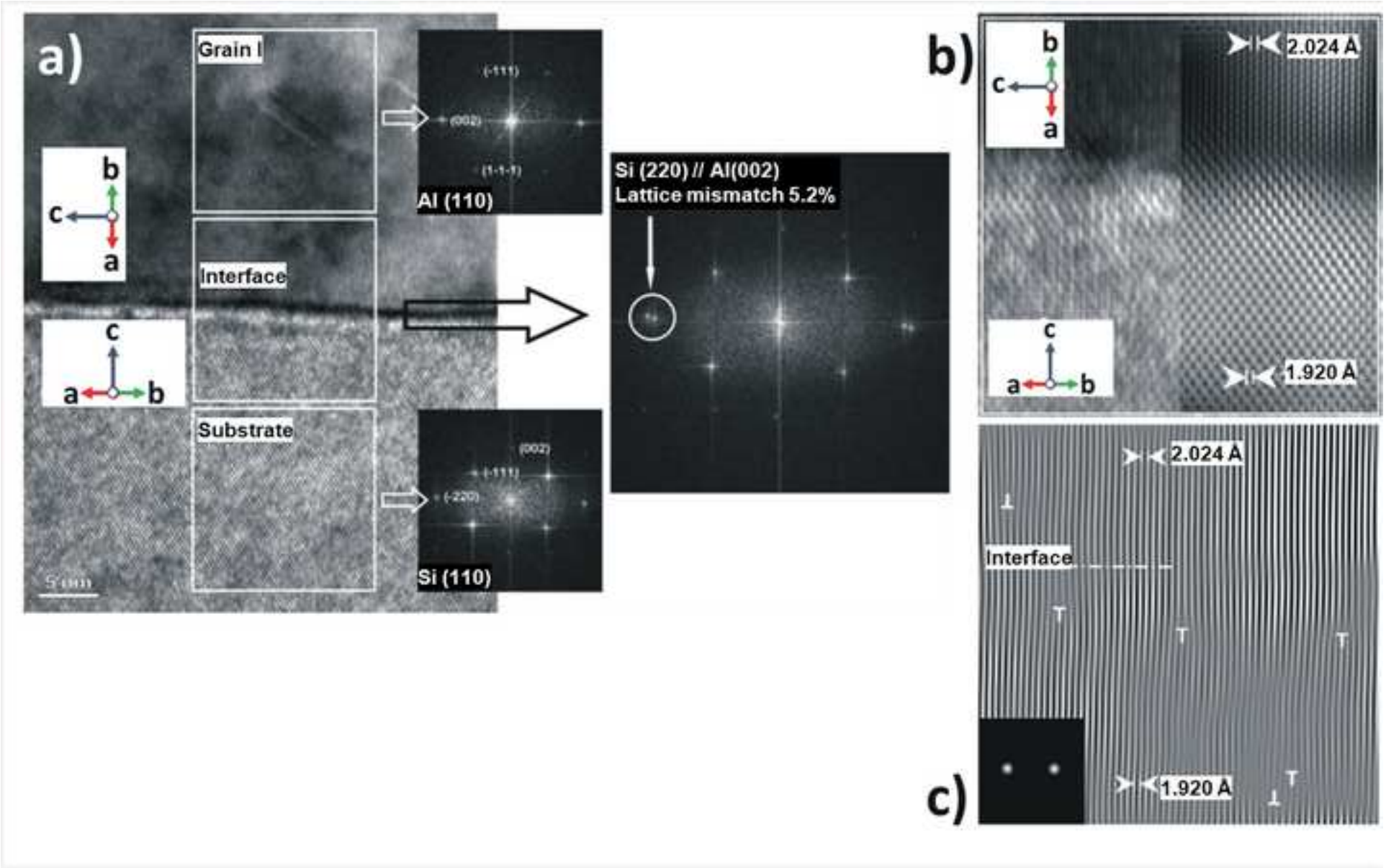

Fig7

Click here to download high resolution image

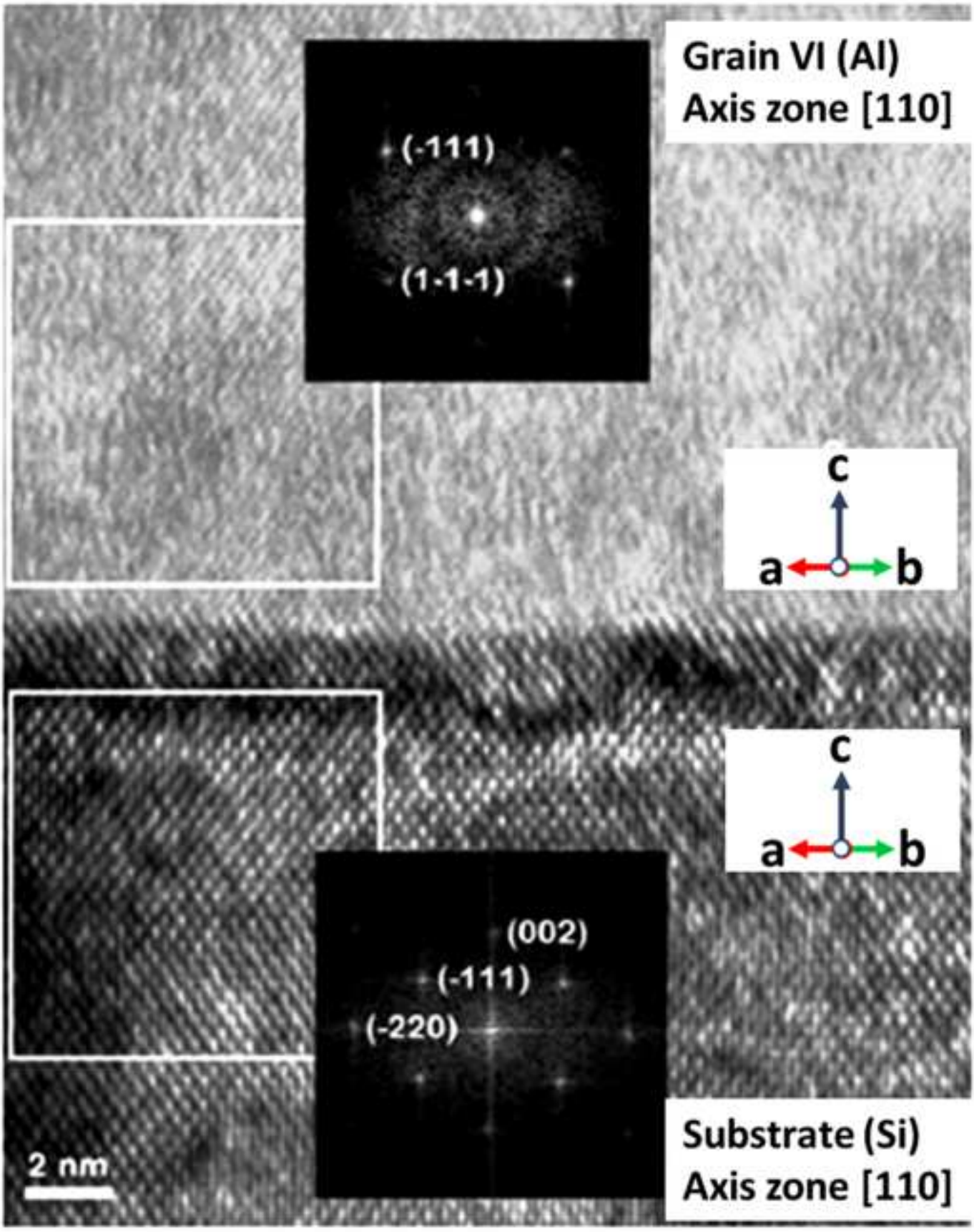

Fig8

Click here to download high resolution image

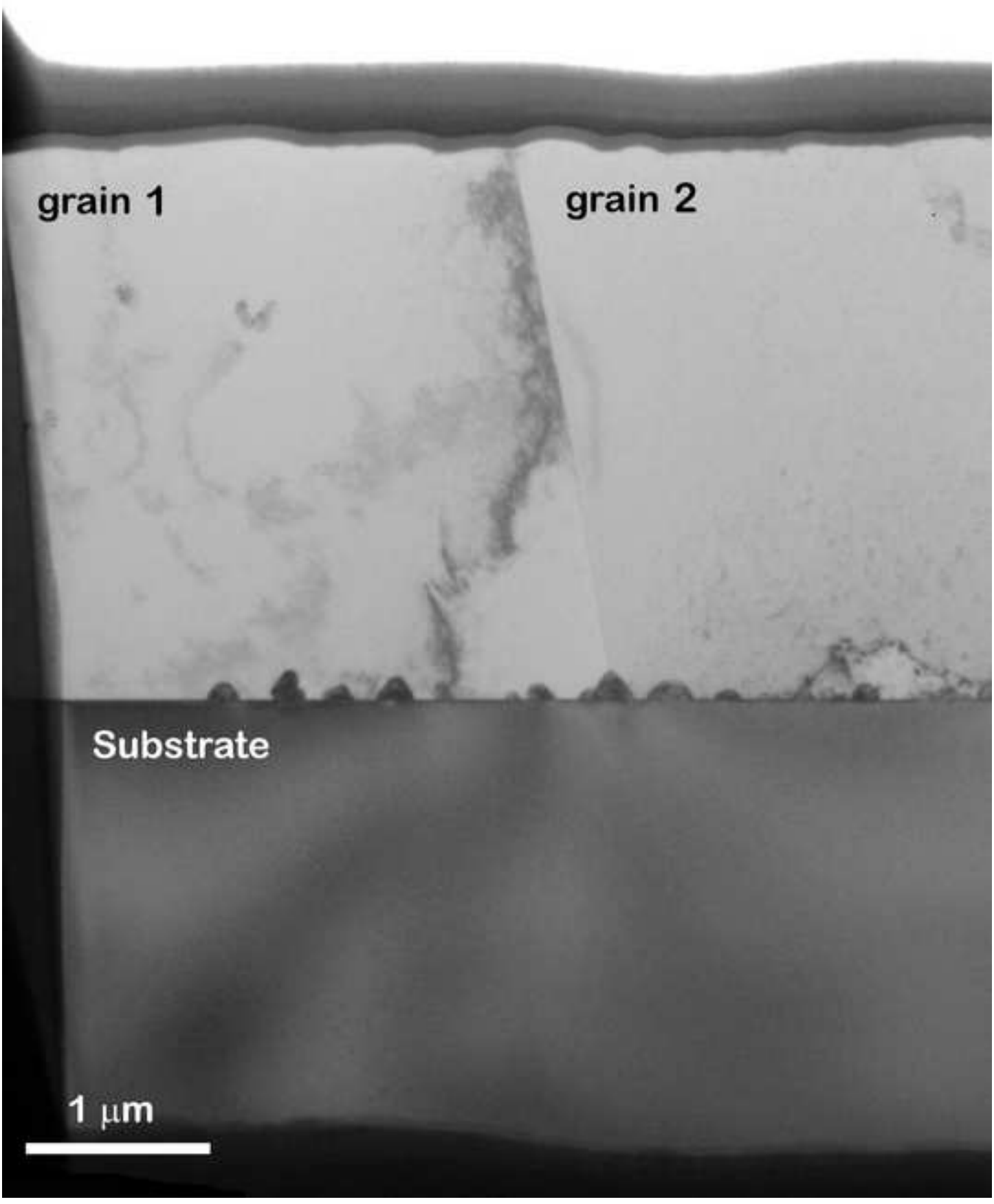

Fig9

Click here to download high resolution image

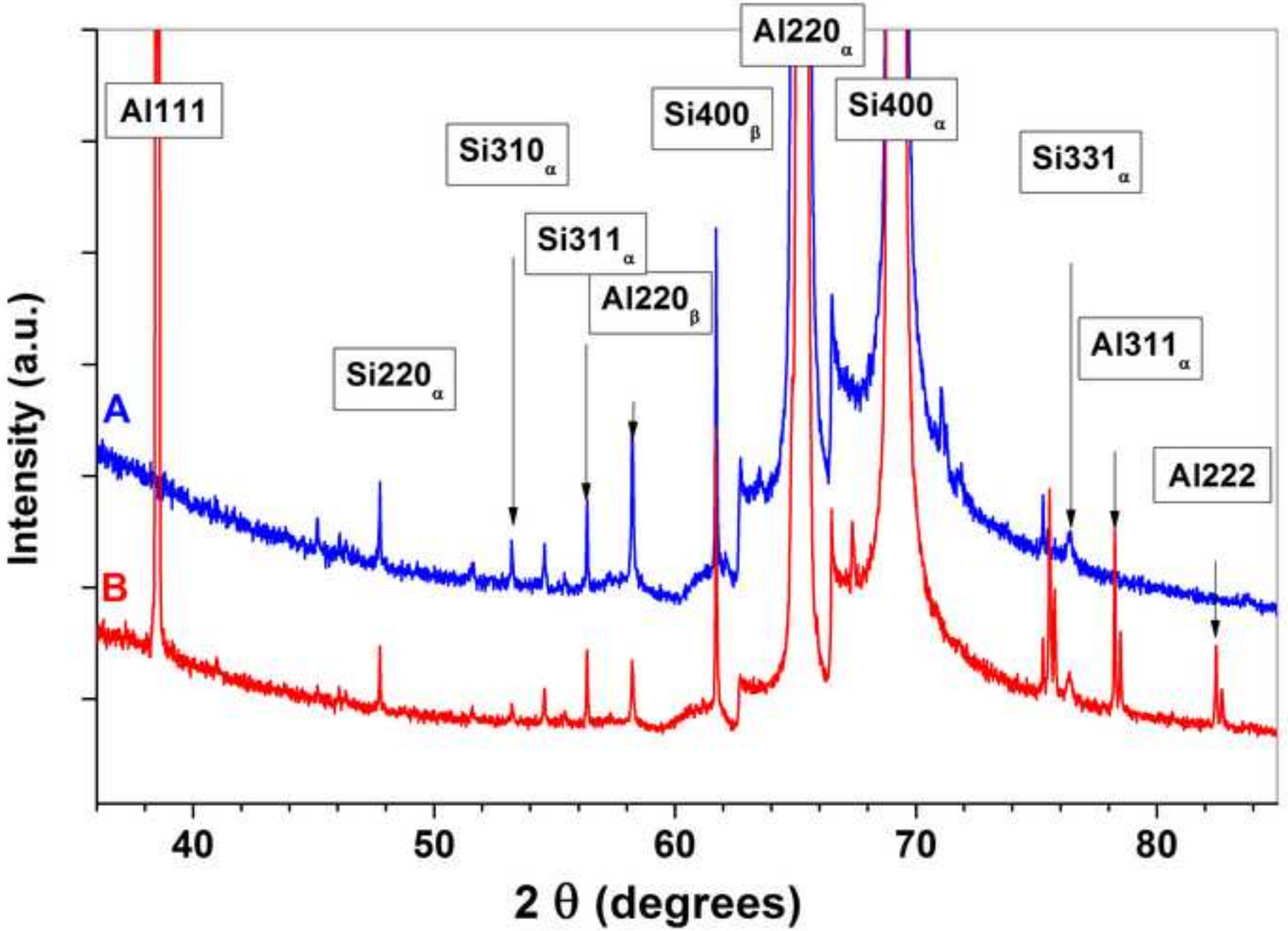

Fig10

Click here to download high resolution image

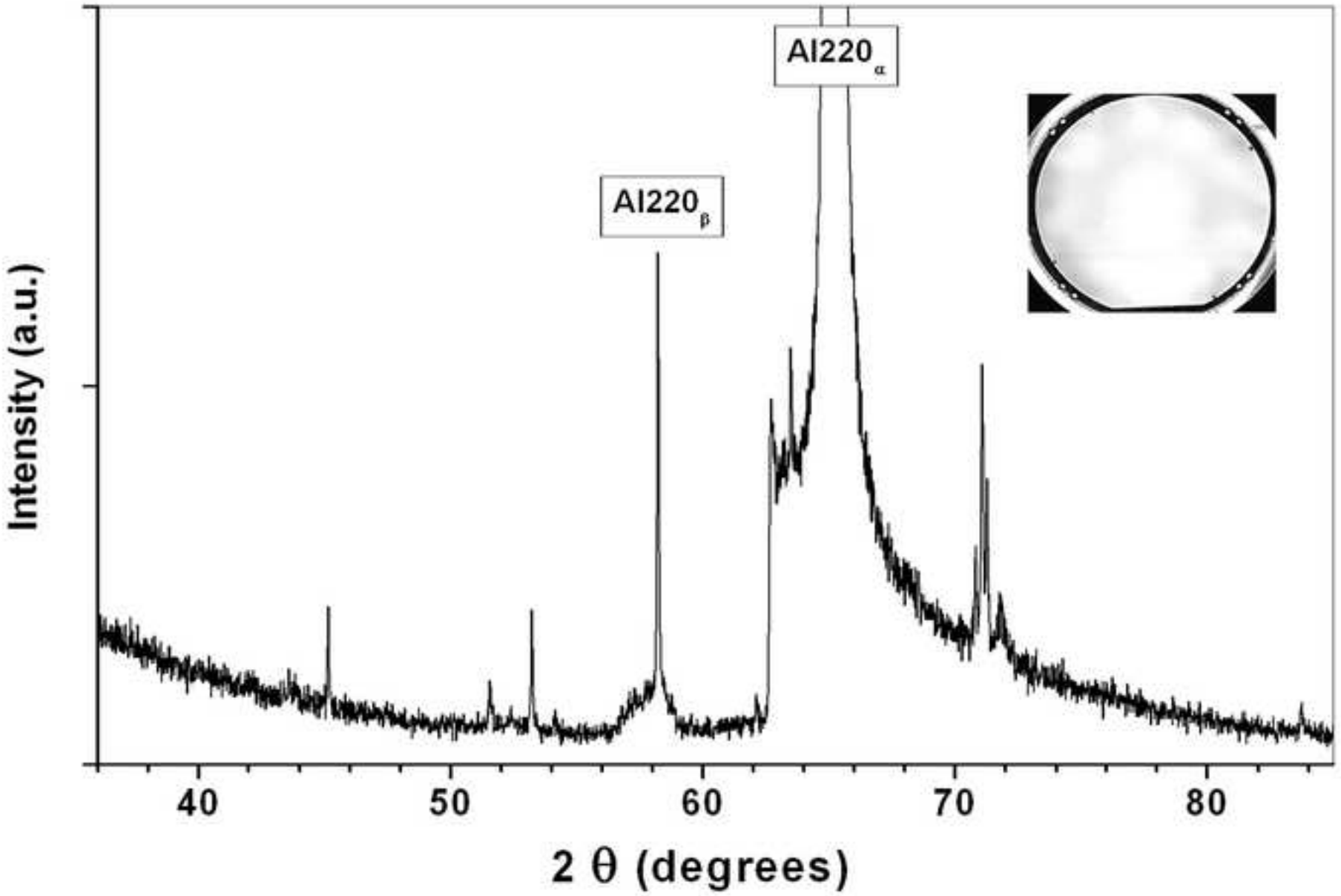

Fig11

Click here to download high resolution image